Large Negative Magnetoresistance Induced by Anionic Solid Solutions in Two-Dimensional Spin-Frustrated Transition Metal Chalcogenides

Yuqiao Guo,[1] Jun Dai,[2] Jiyin Zhao,[1] Changzheng Wu,[1,*] Dianqi Li,[1] Lidong Zhang,[3] Wei Ning,[4] Mingliang Tian,[4] Xiao Cheng Zeng,[2,1] and Yi Xie[1]

[1]*Hefei National Laboratory for Physical Sciences at Microscale and Collaborative Innovation Center of Chemistry for Energy Materials, University of Science and Technology of China, Hefei, Anhui 230026, China*

[2]*Department of Chemistry, University of Nebraska—Lincoln, Lincoln, Nebraska 68588, USA*

[3]*National Synchrotron Radiation Laboratory, University of Science and Technology of China, Hefei, Anhui 230029, China*

[4]*High Magnetic Field Laboratory, Chinese Academy of Science, Hefei, Anhui 230031, China*

(Received 22 June 2014; published 6 October 2014)

We report an anionic solid solution process that induces frustrated magnetic structures within two-dimensional transition metal chalcogenides, which leads to huge negative magnetoresistance effects. Ultrathin nanosheets of $TiTe_{2-x}I_x$ solid solutions, which are a new class of inorganic two-dimensional magnetic material, exhibit negative magnetoresistance with a value of up to −85%, due to the spin-dependent scattering effects of local Ti^{3+} $3d^1$ moments that are antiferromagnetically coupled. Moreover, $TiTe_{2-x}I_x$ serials show unique transport behaviors with continuous evolution from metallic to semiconducting states. We anticipate that anionic doping will be a powerful tool for optimizing the intrinsic physical properties of two-dimensional transition metal chalcogenide system.

DOI: 10.1103/PhysRevLett.113.157202 PACS numbers: 75.47.-m, 73.90.+f, 74.20.Pq

The giant magnetoresistance (GMR) effect, which is a significant change in electrical resistance under an external magnetic field, has revolutionized the sensitivity of magnetic read heads, allowing for dramatic miniaturization of electronics over the past few decades [1,2]. Given the rapid pace at which this field is advancing [3,4], finding nonartificial low-dimensional building blocks with even better intrinsic magnetoresistance (MR) is essential for the sustainability of this burgeoning technology. Because of the planar confined electronic structures and analogous dimensionality of GMR films, two-dimensional nanomaterials, such as graphene, and other inorganic layered materials have been utilized based on their magnetotransport properties for many intriguing spintronic applications [5–9]. Promising room temperature MR effects have been realized in graphene nanoribbons [6]. However, the measured MR in graphene decays rapidly as the ribbon width increases. In addition, graphene itself is nonmagnetic, and the MR effect is attributed to the marginal edge effect of the complexly processed nanoribbons [8,9]. In this regard, inorganic layered nanomaterials, which provide a variety of optional elements and structures in their lattice frameworks, hold great promise for regulating intrinsic magnetoelectric properties [10–13]. Among these materials, layered transition metal chalcogenides (TMCs) offer a variety of transition metal atom coordinations and oxidation states that exhibit exotic two-dimensional characteristics, such as half-metallic magnetism [11], superconductivity [12], and charge density waves [13]. Therefore, developing two-dimensional nanomaterials for next-generation spintronics can benefit from magnetoelectric modulation in two-dimensional TMCs that extends beyond the graphene paradigm.

Despite recent progress in TMCs, there are still substantial challenges involved in integrating electronic and magnetic properties in two-dimensional sandwich structures to meet various technological requirements. Magnetic doping is the conventional method for modulating magnetic behavior. However, employing magnetic cation doping in layered TMC materials is not desirable from a structural standpoint. As in layered sandwich structures, the negatively charged chalcogen elements are exposed on the outer surfaces [14]. When doping with positive magnetic cations, they tend to gather in the interlayer space due to the electrostatic attraction between the doped cations and the surface chalcogen anions, thereby forming intercalated compounds that are very difficult to exfoliate to the two-dimensional nanomaterials [15,16].

Anionic doping provides a new and intriguing platform for regulating the properties of TMCs. By active control and manipulation of the charge and spin degrees of the transition metal within the framework of the two-dimensional structure, anionic doping can regulate the transport and magnetic properties, thereby providing materials with unique spin-related effects. Titanium ditelluride ($TiTe_2$), which is a typical layered TMC material, is composed of triangularly packed layers of the transition metal Ti sandwiched between two Te layers [17]. Because of the perfect size compatibility between iodine (I^-, 2.20 Å) and tellurium (Te^{2-}, 2.21 Å) [18], I^- can be easily introduced into the anionic Te^{2-} site of the $TiTe_2$ lattice to form a $TiTe_{2-x}I_x$ anionic solid solution

system. On the one hand, the electronegativity of I (2.66) is higher than that of Te (2.12) [19], causing more electrons to localize for energy band regulation by tuning the doping content. On the other hand, the anion substitution induces considerable Ti^{3+} formation with the unpaired $3d^1$ electron configuration providing new opportunities to introduce intrinsic magnetic behavior. Therefore, anionic doping offers the exciting potential to regulate the band structure and tune the magnetic properties of two-dimensional TMC materials.

In this Letter, we experimentally demonstrate that an anionic solid solution method can induce a magnetic response and band gap within two-dimensional TMCs, leading to huge negative MR effects. An excess iodine-molecular transport reaction afforded an unprecedentedly large I/Te ratio of 1:1, forming a $TiTe_{2-x}I_x$ anion solid solution system. As expected, our halide-doped TMC material exhibited intrinsic negative MR as high as −85% (5 T, 10 K), which is even superior to the initial GMR Fe/Cr multilayer superlattice of about −20% (5 T, 10 K) [20], representing a huge intrinsic MR effect in two-dimensional TMCs.

Pristine $TiTe_{2-x}I_x$ crystals were obtained using the iodine vapor transport method and were characterized using the XRD, Raman spectroscopy, and XPS, which provided the evidence that iodine was successfully doped into $TiTe_2$ forming the $TiTe_{2-x}I_x$ single crystal solid solution. Density functional theory (DFT) calculations based on Becke's three-parameter Lee-Yang-Parr functional (B3LYP) level were performed to understand the synthesis process. These calculations confirmed that TiTeI can be synthesized and that it was thermodynamically stable. (The detailed preparation and characterization of bulk $TiTe_{2-x}I_x$ single crystals are described in Figs. S1 and S2 of the Supplemental Material [21–28].) The serial characterizations confirmed that the ingredient I and Te atoms were randomly located in the intralayer lattice sites forming $TiTe_{2-x}I_x$ solid solutions.

Ultrathin $TiTe_{2-x}I_x$ nanosheets were obtained using standard mechanical peeling and transferring processes [29,30]. Polarizing microscopy was used to isolate the as-exfoliated ultrathin sheets. Figs. 1(a) and 1(b) show high-resolution XPS spectra for the Ti $2p$ and I $3d$ regions of the TiTeI ultrathin nanosheet. The peaks at 456.3 and 462.2 eV can be attributed to the doublet peaks of Ti^{3+}. The obvious doublet peaks at 618.6 and 630.1 eV can be assigned to I^-. The XPS results demonstrate that iodine was successfully doped into $TiTe_2$ with well-controlled valent states for Ti. The thickness of the nanosheet was quantitatively evaluated using tapping-mode atomic force microscopy. A representative AFM image [Fig. 1(c)] shows that the thickness of the exfoliated nanosheet is ~7.8 nm, which indicates that the nanosheet is composed of approximately 12 Te(I)-Ti-Te(I) sandwich layers. Figures 1(d) and 1(e) show HRTEM images and a schematic diagram of TiTeI viewed down the [001] zone axis. The patterns clearly

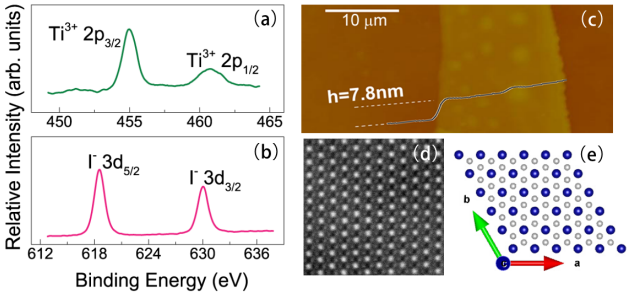

FIG. 1 (color online). (a),(b) High-resolution XPS spectra of the Ti $2p$ and I $3d$ regions of the TiTeI nanosheet. (c) Tapping-mode AFM image of the exfoliated TiTeI nanosheet. (d) HRTEM image of TiTeI viewed down the [001] zone axis. (e) Schematic diagram of 1T-TiTeI crystal structure.

demonstrate that the hexagonal crystals with Ti ions are triangularly arranged in an isostructural configuration with pristine 1T-$TiTe_2$. Together, these results demonstrate that the iodine was localized in the lattice sites of the intralayer sites of the Te-Ti-Te crystal to form a 1T-TiTeI structure.

A large amount of iodine substitution allows valence engineering of the titanium from Ti^{4+} to Ti^{3+} with unpaired electrons, which offers a source for inducing the intrinsic magnetic properties in the two-dimensional structure. Temperature-dependent magnetizations were fitted to the Curie-Weiss (C-W) law: $\chi = C/(T-\theta)$, where C is the Curie constant, as shown in Figs. 2(a) and 2(b). The high-temperature data were well fitted by the C-W law, indicating their paramagnetic (PM) behaviors. However, there were clear downward deviations in the inverse magnetization from

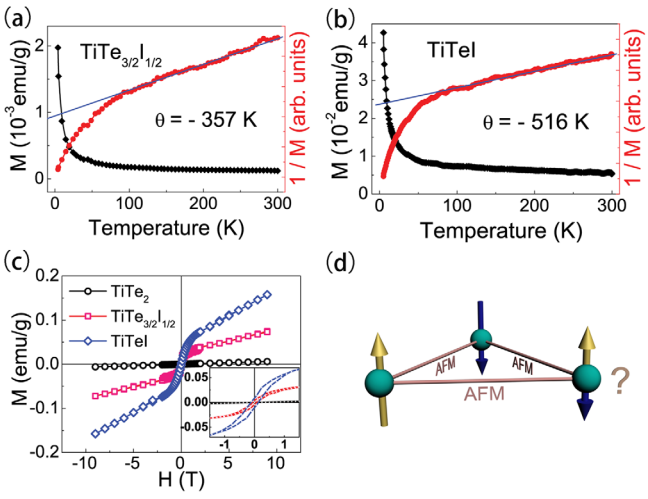

FIG. 2 (color online). (a),(b) The temperature-dependent magnetizations and inverse magnetizations for $TiTe_{3/2}I_{1/2}$ and TiTeI, respectively. The solid lines represent the C-W fitting lines. (c) Field-dependent magnetizations at 10 K for $TiTe_2$, $TiTe_{3/2}I_{1/2}$, and TiTeI. The inset shows an enlarged view of the low magnetic field region. (d) Schematic representation of three AFM-coupled spins on triangular lattice forming frustrated configuration.

the C-W law at temperature lower than about 80 K, indicating the onset of the magnetic correlation. The Weiss temperature (θ) was obtained from fitting the high-temperature PM regime with the C-W law. The large negative θ ($TiTe_{3/2}I_{1/2}$: −357 K, TiTeI: −516 K) indicated antiferromagnetic (AFM) coupling between the neighboring spins. Figure 2(c) shows the magnetic field-dependent magnetization at 10 K, from which we can observe that the magnetization of TiTeI shows hysteresis under low fields [as shown in the inset of Fig. 2(c)], whereas it is linear and nonsaturated under high fields. The nonsaturated character indicates an AFM ground state in iodine-doped system. Similar high-field nonsaturated, low-field hysteresis loops have been reported for the antiferromagnetic coupling of hexagonal and triangular structures, such as manganite $RMnO_3$ (R = Ho, Tb, Dy, Y, etc.) [31] and ferrites [32], where geometrical frustration induced spiral or canted antiferromagnetic ordering was account for the nonsaturated hysteresis loop [33,34]. Considering the triangular topological configuration and antiferromagnetic coupling of the nearest-neighboring Ti^{3+} ions, as schematically shown in Fig. 2(d), we proposed that the magnetic state for TiTeI is geometrically frustrated antiferromagnetism at 10 K (see more analysis in Fig. S3 of the Supplemental Material [21]). Antiferromagnetic coupling of Ti^{3+} ions has also been observed in $LaTiO_3$ and $PrTiO_3$; this observation supports the antiferromagnetic exchange interaction between the magnetic Ti^{3+} ions in TiTeI [35].

The Ti^{3+} ions with $3d^1$ unpaired electrons are located in the intralayer lattice, which is the pathway for the current carriers that are responsible for conductivity. Thus, the scattering effect between the local magnetic moment and the carrier electrons plays a prominent role in the magnetic-transport behavior. The magnetic-transport properties of the ultrathin nanosheets were investigated using standard four probe transport measurements in a commercial apparatus (Quantum Design, PPMS). The direction of the applied magnetic field was perpendicular to the sample surface, and the dc resistivity was measured between 10 and 300 K under an applied field of up to 5 T. Figure 3(a) shows the temperature dependence of the resistivity for a pristine $TiTe_2$ ultrathin nanosheet under different magnetic fields. Similar to the results reported for metallic bulk $TiTe_2$, the nanosheet counterpart had a positive temperature coefficient of resistivity, which can be attributed to a moderate electron-phonon interaction in the usual quasiparticle gas model [36]. The ordinary positive MR effect of 2% under an external magnetic field originated from the electron cyclotron orbital effect due to the Lorentz force. Figure 3(b) shows the temperature and magnetic field dependences of

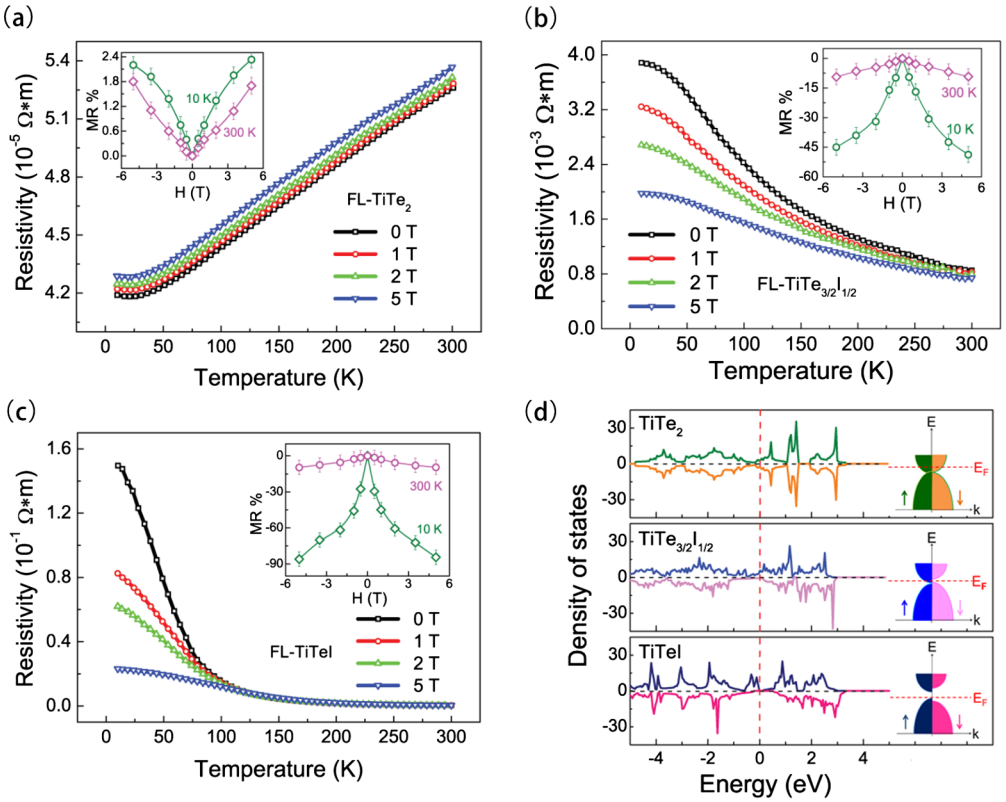

FIG. 3 (color online). Magnetotransport behavior of a few-layer (FL) thick $TiTe_{2-x}I_x$ nanosheet. (a)–(c) The temperature-dependent resistivity under various magnetic fields for $TiTe_2$, $TiTe_{3/2}I_{1/2}$, and TiTeI. Insets: Magnetic field dependence of the MR for samples at 10 and 300 K. The MR was calculated by $MR\% = [R(H) - R(0)]/R(0)$. (d) DOS diagram of the monolayer $TiTe_2$, $TiTe_{3/2}I_{1/2}$, and TiTeI optimized structures.

the resistivity for a $TiTe_{3/2}I_{1/2}$ ultrathin nanosheet. After doping with iodine, the sample followed a completely different tendency from the metallic behavior of pristine $TiTe_2$ (i.e., the resistance increased as the temperature decreased). However, the magnitude of the increase was not strongly dependent on temperature [37]. Thus, the phenomenon was considerably different from typical semiconducting behavior in which the resistivity exponentially increases as the temperature decreases. As shown in Fig. 3(c), as the iodine doping content was further increased, the resistivity of the TiTeI ultrathin nanosheet rapidly increased with decreasing temperature, indicating a gap opening in this newly synthetized two-dimensional material. In particular, DFT-calculated DOS of the optimized monolayers of $TiTe_2$, $TiTe_{3/2}I_{1/2}$, and TiTeI [presented in Fig. 3(d)] clearly show that with an increase in the ratio of I/Te, $TiTe_{2-x}I_x$ series undergo transitions from metal to half-metal to semiconducting states. The DOS near the Fermi energy level was primarily contributed by the Ti d states.

Furthermore, the resistivity of the ultrathin TiTeI nanosheet was greatly suppressed under an external magnetic field, and the value of MR for the TiTeI ultrathin nanosheet reached as high as −85% (5 T, 10 K), inset of Fig. 3(c), representing the first huge MR effect among the TMC materials. The MR value was even larger than that of the first reported GMR material, the Fe/Cr/Fe structure (−20% at 5 T, 10 K), which is the core component of the most famous commercial data reader [20]. Considering the theoretical limit for a negative MR of −100%, our TiTeI with MR value of −85% represents a very large negative MR effect.

For solids with magnetic coupling, the magnetic-transport behaviors are strongly related to the spin arrangements under an external magnetic field [38]. An antiferromagnetic coupling that can induce spin-dependent scattering or tunneling effects should lead to MR behavior. For example, in perovskite $CaMnO_{3-\delta}$ and La_2NiMnO_6, antiferromagnetic domain scattering effects and external field-tunable spin arrangements produced their large negative MR [39,40]. In our TiTeI sample, the transport data can be divided into two regions according to the magnetic C-W fitting: in a high-temperature PM region, $\rho - T$ obeyed the Arrhenius law and the value of MR was relatively small. However, in the low-temperature region, where the unpaired spins had antiferromagnetic order, the $\rho - T$ data departed from the thermally activated model and the MR increased rapidly with decreasing temperature [shown in Fig. 4(a)]. This result suggests that antiferromagnetic coupling of spins in TiTeI directly influences the conduction of the carriers. Moreover, the magnetism analysis confirmed the existence of frustrated antiferromagnetic states in the TiTeI. Thus, the intrinsically frustrated antiferromagnetism acted as a spin-dependent scattering barrier, resulting in the MR effect.

Considering the frustrated antiferromagnetic coupling of the Ti^{3+} moments and the band gap opening, we hypothesized that the huge MR of the TiTeI ultrathin nanosheet

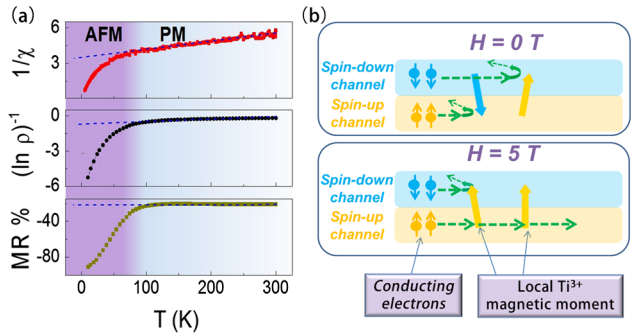

FIG. 4 (color online). Mechanism for the negative MR effect. (a) (top to bottom) Temperature-dependent inverse susceptibility ($1/\chi$), fitted resistivity (ρ), and MR for the TiTeI. Here, the resistivity data were fitted using the thermally activated model: $\rho = \rho_0 \exp(E/k_B T)$, where E is the activation energy, ρ_0 and k_B are constants. (b) Schematic diagram of the spin-dependent scattering between the conducting electrons and the local Ti^{3+} magnetic moment in the ultrathin TiTeI.

was due to spin-dependent scattering of the conducting electrons on the local magnetic moments. During the conduction process, the conducting electrons move collectively throughout the layers in the direction of the electric field to form the electric current. According to the two-current model of magnetic materials, the conduction occurs in parallel through two spin channels (spin-up and spin-down conducting electrons) with magnetic scattered intensity exerted upon the conducting electrons depending on the relative orientations between spins and the local magnetic moments. Scattering is weakest when they are parallel and strongest when they are antiparallel [41–43]. In the TiTeI nanosheets, the local Ti^{3+} magnetic moments, which are antiferromagnetically coupled, act as strong scattering centers for both spin-up and spin-down electrons without magnetic field, as illustrated in the upper portion of Fig. 4(b). However, after applying a magnetic field, the local Ti^{3+} magnetic moments arrange parallel to the external magnetic field direction decreasing the scattering probability of one of the spin channel electrons as illustrated in the bottom portion of Fig. 4(b). The consequence of alignment of the Ti^{3+} magnetic moment is a reduction in the equivalent all-in resistivity by short circuiting, which is consistent with the observed negative MR effect. Of note, the similar MR effect was also observed in much thicker TiTeI samples, as described in Fig. S4 of the Supplemental Material [21], further supporting that negative MR effects observed in the TiTeI samples were mainly depended on iodine-doping induced magnetic behavior of Ti^{3+} moment and the energy gap opening, independent of thickness to some extent.

In summary, anionic doping was utilized to achieve frustrated magnetic structures in TMCs. $TiTe_{2-x}I_x$ anion solid solutions simultaneously achieved band gap openings and intrinsic magnetic responses in the two-dimensional materials. These new TiTeI ultrathin nanosheets provide

huge MR effects of up to 85%, representing the first intrinsic negative MR effect for TMC materials. Furthermore, the new anion-doped $TiTe_{2-x}I_x$ solid solutions exhibited successive electronic phase transitions from metal to semiconducting states through tuning the iodine content, which provides the possibility of producing custom-designed building blocks with a variety of energy gaps in two-dimensional materials. Thus, anionic doping is a powerful tool for engineering the intrinsic properties of two-dimensional confined systems.

We thank Dr. S. M. Zhou (HFNL, USTC) for the helpful discussion of the crystal structure. This work was financially supported by the National Natural Science Foundation of China (Grants No. 21222101, No. U1432133, No. 11132009, No. 21331005, No. 11321503, and No. J1030412), Chinese Academy of Science (XDB01010300), and the Fundamental Research Funds for the Central Universities (WK2060190031, WK2060190027, WK2310000024).

*Corresponding author.
czwu@ustc.edu.cn

[1] M. N. Baibich, J. M. Broto, A. Fert, F. Nguyen Van Dau, F. Petroff, P. Etienne, G. Creuzet, A. Friederich, and J. Chazelas, Phys. Rev. Lett. **61**, 2472 (1988).
[2] A. Fert, Rev. Mod. Phys. **80**, 1517 (2008).
[3] C. Chappert, A. Fert, and F. Nguyen Van Dau, Nat. Mater. **6**, 813 (2007).
[4] B. Behin-Aein, D. Datta, S. Salahuddin, and S. Datta, Nat. Nanotechnol. **5**, 266 (2010).
[5] W. Y. Kim and K. S. Kim, Nat. Nanotechnol. **3**, 408 (2008).
[6] J. Bai, R. Cheng, F. X. Xiu, L. Liao, M. S. Wang, A. Shailos, K. L. Wang, Y. Huang, and X. F. Duan, Nat. Nanotechnol. **5**, 655 (2010).
[7] W. Yang, G. R. Chen, Z. W. Shi, C.-C. Liu, L. C. Zhang, G. B. Xie, M. Cheng, D. M. Wang, R. Yang, D. X. Shi, K. Watanabe, T. Taniguchi, Y. G. Yao, Y. B. Zhang, and G. Y. Zhang, Nat. Mater. **12**, 792 (2013).
[8] F. Muñoz-Rojas, J. Fernández-Rossier, and J. J. Palacios, Phys. Rev. Lett. **102**, 136810 (2009).
[9] R. Ribeiro, J.-M. Poumirol, A. Cresti, W. Escoffier, M. Goiran, J.-M. Broto, S. Roche, and B. Raquet, Phys. Rev. Lett. **107**, 086601 (2011).
[10] Q. H. Wang, K. Kalantar-Zadeh, A. Kis, J. N. Coleman, and M. S. Strano, Nat. Nanotechnol. **7**, 699 (2012).
[11] W.-H. Xie, Y.-Q. Xu, B.-G. Liu, and D. G. Pettifor, Phys. Rev. Lett. **91**, 037204 (2003).
[12] B. Sipos, A. F. Kusmartseva, A. Akrap, H. Berger, L. Forró, and E. Tutiš, Nat. Mater. **7**, 960 (2008).
[13] M. M. May, C. Brabetz, C. Janowitz, and R. Manzke, Phys. Rev. Lett. **107**, 176405 (2011).
[14] M. Chhowalla, H. S. Shin, G. Eda, L.-J. Li, K. P. Loh, and H. Zhang, Nat. Chem. **5**, 263 (2013).
[15] W. Z. Hu, G. T. Wang, R. W. Hu, C. Petrovic, E. Morosan, R. J. Cava, Z. Fang, and N. L. Wang, Phys. Rev. B **78**, 085120 (2008).
[16] A. H. Thompson, Phys. Rev. Lett. **40**, 1511 (1978).
[17] D. K. G. de Boer, C. F. van Bruggen, G. W. Bus, R. Coehoorn, C. Haas, G. A. Sawatzky, H. W. Myron, D. Norman, and H. Padmore, Phys. Rev. B **29**, 6797 (1984).
[18] R. D. Shannon, Acta Crystallogr. Sect. A **32**, 751 (1976).
[19] A. L. Allred, J. Inorg. Nucl. Chem. **17**, 215 (1961).
[20] M. A. M. Gijs and M. Okada, Phys. Rev. B **46**, 2908 (1992).
[21] See Supplemental Material at http://link.aps.org/supplemental/10.1103/PhysRevLett.113.157202, which includes Refs. [22–28], for detailed preparation and crystal structural information, magnetic and thickness dependent properties of the samples.
[22] C. W. Lin, X. J. Zhu, J. Feng, C. Z. Wu, S. L. Hu, J. Peng, Y. Q. Guo, L. L. Peng, J. Y. Zhao, J. L. Huang, J. L. Yang, and Y. Xie, J. Am. Chem. Soc. **135**, 5144 (2013).
[23] A. V. Shevelkov, E. V. Dikarev, R. V. Shpanchenko, B. A. Popovkin, J. Solid State Chem. **114**, 379 (1995).
[24] G. M. Sheldrick, *SHELXL-97, program for x-ray crystal structure refinement* (Göttingen University, Germany, 1997).
[25] M. Hangyo, S.-I. Nakashima, and A. Mitsuishi, Ferroelectrics **52**, 151 (1983).
[26] M. Staruch, D. Violette, and M. Jain, Mater. Chem. Phys. **139**, 897 (2013).
[27] S. Jin, T. H. Tiefel, M. McCormack, R. A. Fastnacht, R. Ramesh, and L. H. Chen, Science **264**, 413 (1994).
[28] X. L. Wang, Y. Du, S. X. Dou, and C. Zhang, Phys. Rev. Lett. **108**, 266806 (2012).
[29] K. S. Novoselov, A. K. Geim, S. V. Morozov, D. Jiang, Y. Zhang, S. V. Dubonos, I. V. Grigorieva, and A. A. Firsov, Science **306**, 666 (2004).
[30] J. Song, F.-Y. Kam, R.-Q. Png, W.-L. Seah, J.-M. Zhuo, G.-K. Lim, P. K. H. Ho, and L.-L. Chua, Nat. Nanotechnol. **8**, 356 (2013).
[31] M. Fiebig, Th. Lottermoser, and R. V. Pisarev, J. Appl. Phys. **93**, 8194 (2003).
[32] R. C. Pullar, Prog. Mater. Sci. **57**, 1191 (2012).
[33] M. Mochizuki and N. Furukawa, Phys. Rev. Lett. **105**, 187601 (2010).
[34] W. B. Wang, J. Zhao, W. B. Wang, Z. Gai, N. Balke, M. F. Chi, H. N. Lee, W. Tian, L. Y. Zhu, X. M. Cheng, D. J. Keavney, J. Y. Yi, T. Z. Ward, P. C. Snijders, H. M. Christen, W. D. Wu, J. Shen, and X. S. Xu, Phys. Rev. Lett. **110**, 237601 (2013).
[35] M. Mochizuki and M. Imada, Phys. Rev. Lett. **91**, 167203 (2003).
[36] J. M. Ziman, *Principles of the Theory of Solids*, 2nd ed. (Cambridge University Press, Cambridge, England, 1972).
[37] X. D. Zhang, J. J. Zhang, J. Y. Zhao, B. C. Pan, M. G. Kong, J. Chen, and Y. Xie, J. Am. Chem. Soc. **134**, 11908 (2012).
[38] H. Y. Hwang, S-W. Cheong, N. P. Ong, and B. Batlogg, Phys. Rev. Lett. **77**, 2041 (1996).
[39] Z. Zeng, M. Greenblatt, and M. Croft, Phys. Rev. B **59**, 8784 (1999).
[40] Y. Q. Guo, L. Shi, S. M. Zhou, J. Y. Zhao, and W. J. Liu, Appl. Phys. Lett. **102**, 222401 (2013).
[41] N. H. Mott, Proc. R. Soc. A **153**, 699 (1936).
[42] R. E. Camley and J. Barnaś, Phys. Rev. Lett. **63**, 664 (1989).
[43] W. H. Butler, X. G. Zhang, D. M. C. Nicholson, and J. M. MacLaren, J. Magn. Magn. Mater. **151**, 354 (1995).